IEEE Access
Multidisciplinary | Rapid Review | Open Access Journal

Received July 24, 2021, accepted August 13, 2021, date of publication August 18, 2021, date of current version August 27, 2021.

Digital Object Identifier 10.1109/ACCESS.2021.3106050

Assessment and Analysis of the Four-Satellite QZSS Precise Point Positioning and the Integrated Data Processing With GPS

XUANPING LI[1], LIN PAN[1,2,3], AND WENKUN YU[1]
[1]School of Geosciences and Info-Physics, Central South University, Changsha 410083, China
[2]State Key Laboratory of Geo-Information Engineering, Xi'an 710054, China
[3]Guangxi Key Laboratory of Spatial Information and Geomatics, Guilin 541004, China

Corresponding author: Lin Pan (linpan@csu.edu.cn)

This work was supported in part by the National Natural Science Foundation of China under Grant 41904030, in part by the Natural Science Foundation of Hunan Province, China, under Grant 2020JJ5706, in part by the State Key Laboratory of Geo-Information Engineering under Grant SKLGIE2019–Z–1–1, in part by the Guangxi Key Laboratory of Spatial Information and Geomatics under Grant 19-050-11-09, and in part by the Fundamental Research Funds for the Central Universities of Central South University under Grant 2021zzts0851.

ABSTRACT The Quasi-Zenith Satellite System (QZSS), which serves Japan and its surrounding areas, is a regional navigation satellite system developed by Japan Aerospace Exploration Agency. The system is now in a four-satellite constellation with preliminary standalone navigation and positioning capabilities. In this paper, the performance of QZSS-only precise point positioning (PPP) in both static and kinematic modes is initially evaluated using the datasets spanning 11 days from 11 tracking stations in Asia-Pacific regions and the final precise orbit and clock products from the analysis centers GFZ and WUM. For completeness, the GPS/QZSS integrated data processing with GFZ and WUM final products as well as the L6E real-time orbit and clock corrections is also analyzed. The results indicate that the static positioning accuracy of QZSS-only PPP is approximately 4, 2 and 15 cm in the east, north and up directions, respectively, and the static convergence time of QZSS-only PPP with WUM and GFZ products can be 75.2, 44.3 and 45.6 min, and 153.5, 201.6 and 162.8 min in the three directions, respectively. As for the QZSS-only kinematic PPP solutions, the re-convergence repeatedly occurs due to limited available satellites. To achieve more reliable solutions, the inter-system bias parameter in GPS/QZSS PPP processing is recommended to be estimated as random walk process or white noise process. The improvement of post-processed GPS/QZSS PPP over GPS-only case is marginal on position accuracies, but can be several minutes on convergence time. Compared with post-processed GPS/QZSS PPP, the real-time one achieves worse position accuracies but comparable convergence time.

INDEX TERMS QZSS, GPS, precise point positioning, inter-system bias.

I. INTRODUCTION

The Quasi-Zenith Satellite System (QZSS) is a regional navigation satellite system, which aims to serve Japan and its surrounding areas. The system is currently in a four-satellite constellation, including three inclined geosynchronous orbit (IGSO) satellites (J01, J02 and J03) and one geostationary orbit (GEO) satellite (J07). QZSS was originally designed as a complementary system for GPS to enhance the navigation and positioning capabilities in mountainous areas and urban canyons of Japan. The launch of the QZSS service was officially announced on November 1, 2018. QZSS is planned to be extended to a seven-satellite system by 2023, so that the positioning, navigation and timing (PNT) services of QZSS itself can be improved.

QZSS broadcasts four signals compatible with GPS on the L1 (1575.42 MHz), L2 (1227.60 MHz) and L5 (1176.45 MHz) bands. After the QZSS satellites were successfully launched, many scholars carried out a detailed analysis on the quality of signals, the accuracy of ephemeris, and the performance of combined positioning with the existing Global Navigation Satellite Systems (GNSSs). Due to

The associate editor coordinating the review of this manuscript and approving it for publication was Venkata Ratnam Devanaboyina.

the high orbital altitude of the QZSS satellites, the carrier-to-noise density ratios of QZSS signals were approximately 1.5–5 dB-Hz less powerful than those of GPS signals. In addition, the code multipath errors on both L1 and L2 bands exhibited similar performance due to the same central frequency of the QZSS and GPS signals [1]. The standard deviations (STDs) of double-difference phase residuals derived from zero-baseline observations of QZSS L1 C/A, L2C, and L5 signals were also comparable to those of the corresponding GPS signals, which were both reported to 0.5–1 mm by Quan *et al.* [2]. Although the QZSS signals adopt the same central frequency as GPS signals, the inter-system bias (ISB) between the two satellite systems was still evident in their combined data processing [3], [4]. Therefore, the performance of GPS/QZSS integrated positioning and navigation will degrade if the influence of ISB is ignored. Xie *et al.* [5] analyzed the satellite clock characteristics of QZSS on a long-term scale, and the frequency stability was 1.98×10^{-13}, 6.59×10^{-14} and 5.39×10^{-14} at an integration time of 100, 1000 and 10,000 s, respectively. Guo *et al.* [6] first performed an assessment on the quality of precise orbit and clock products from different Multi-GNSS Experiment (MGEX) analysis centers (CODE/JAXA/TUM) for the first QZSS satellite (J01) using the datasets during 2013–2015. The consistency of precise orbit and clock products among different analysis centers for this QZSS satellite was 0.2–0.4 m and 0.4–0.8 ns, respectively. Subsequently, Li *et al.* [7] further evaluated the quality of precise ephemeris under the MGEX analysis centers for all the four QZSS satellites. They found that the orbit comparison of the J07 satellite in the along-track component was 256.4 cm between GFZ and WUM products, and the clock difference of the J01 satellite reached 1 ns between GFZ and other agencies, indicating that the strategies of precise orbit determination (POD) and precise clock estimation (PCE) for QZSS satellites need to be strengthened by the MGEX analysis centers. Based on the satellite laser ranging (SLR) validations, the quality of multi-system combined orbits generated with the individual products from MGEX and international GNSS service (IGS) analysis centers was evaluated by Sośnica *et al.* [8], and it was determined that the mean STDs of SLR residuals for QZSS satellites were 72 mm, while the corresponding statistics of BDS-2 GEO and IGSO satellites were reported to 87 and 51 mm, respectively. By applying new satellite metadata for a priori box-wing solar radiation pressure model, the three-dimensional (3D) root mean squares (RMSs) of orbit overlaps and the STDs of clock overlaps for the J02 satellite were reduced by 13.8% and 20.5%, respectively, when compared to the ECOM2 model [9].

Many scholars carried out the researches on the QZSS precise positioning, but they mainly focused on the contribution of QZSS to GNSS data processing, for example, GPS/QZSS PPP [10], BDS-2/BDS-3/QZSS PPP [11], and GPS/BDS-2/GLONASS/Galileo/QZSS PPP [12]. Regarding the research of PPP ambiguity-fixed solutions, Hu *et al.* [13] generated the fractional cycle biases (FCBs) of QZSS satellites using CODE precise ephemeris, and the mean STDs of wide-lane and narrow-lane QZSS FCBs were 0.008 and 0.010 cycles, respectively, which were even more stable than GPS FCBs (0.019 and 0.021 cycles) and BDS-2 FCBs (0.015 and 0.057 cycles). The QZSS extra-wide-lane, wide-lane and narrow-lane FCBs were also obtained from the uncombined triple-frequency observations [14], and their mean STDs were 0.003, 0.018 and 0.026 cycles, respectively. Besides the four PNT signals (L1 C/A, L1C, L2C and L5), two enhanced services for GNSS are also provided by QZSS satellites, including the sub-meter level and the centimeter level augmentation services provided by the L1-SAIF signal and LEX signal, respectively. Following Choy *et al.* [15], using the satellite orbit and clock corrections delivered by the QZSS LEX signal, the static position accuracies of GPS PPP after a processing time of two hours were 2.9, 1.2 and 2.6 cm in the east, north and up directions, respectively. The derived GPS real-time PPP results were only slightly worse than those with the IGS real-time stream CLK11, indicating that the accuracy of the QZSS augmentation service is adequate for real-time PPP applications. The enhanced information on the QZSS LEX signal comes from multi-GNSS advanced demonstration tool for orbit and clock analysis (MADOCA), and the positioning accuracy of GPS kinematic PPP using the MADOCA real-time precise products was 4.9, 4.2 and 11.7 cm in the three directions, respectively [16].

With the formation of the four-satellite constellation, the single-system positioning of QZSS becomes possible. QZSS is expected to be extended to a seven-satellite constellation, and the satellite system users will be increasingly interested in its standalone positioning performance. The QZSS-only single point positioning (SPP) based on four available satellites was first analyzed in Li *et al.* [17], and the positioning accuracies were 5.70, 3.20 and 6.99 m in the east, north and up directions, respectively, which were worse than those of GPS-only SPP with a statistic of 0.77, 1.16 and 3.23 m in the three directions, respectively. The QZSS-only real-time kinematic (RTK) positioning was implemented for the first time in Zaminpardaz *et al.* [18], and the instantaneous ambiguity resolution and the centimeter-level positioning results were achieved. However, the positioning performance of QZSS-only PPP has not been reported.

In this study, we carry out the static and kinematic PPP processing with four available QZSS satellites to analyze its standalone positioning performance. As QZSS was originally designed as a complementary system for GPS to enhance the position determination over Japan, the QZSS/GPS integrated data processing is also conducted. The structure of this paper is described as follows. The paper starts with the observation model of PPP and the dynamic model of ISB, and then the datasets and processing strategies are described. Next, the results are presented and discussed. In the last section, a summary of the main conclusions is provided.

II. OBSERVATION MODEL FOR QZSS-ONLY, GPS-ONLY AND GPS/QZSS PPP

To eliminate the influence of the first-order ionospheric delay, the dual-frequency code and phase observations are often used to form the ionospheric-free (IF) combination in PPP. The L1/L2 dual-frequency IF combined observations of QZSS or GPS can be described as follows:

$$\begin{cases} P_{IF} = \rho + c\mathrm{d}t_r - c\mathrm{d}t^s + T + b_{r,IF} - b^s_{IF} + \varepsilon_{P,IF} \\ L_{IF} = \rho + c\mathrm{d}t_r - c\mathrm{d}t^s + T + \lambda_{IF} \\ \qquad \cdot(N_{IF} + B_{r,IF} - B^s_{IF}) + \varepsilon_{L,IF} \end{cases} \tag{1}$$

where P_{IF} and L_{IF} are code and phase observations, respectively, ρ is the geometric distance between the receiver and the satellite, $c\mathrm{d}t_r$ and $c\mathrm{d}t^s$ are the receiver and satellite clock offsets, respectively, T denotes the slant tropospheric delay, λ_{IF} is the wavelength of the IF observations, $b_{r,IF}$ and b^s_{IF} denote the receiver-dependent and satellite-dependent IF combination of uncalibrated code delays (UCDs), respectively, N_{IF} is the phase ambiguity, $B_{r,IF}$ and B^s_{IF} denote the receiver-dependent and satellite-dependent IF combination of uncalibrated phase delays (UPDs), respectively, which will be absorbed into the phase ambiguity parameters due to the linear dependence of these terms, and $\varepsilon_{P,IF}$ and $\varepsilon_{L,IF}$ are the measurement noises grouped with multipath errors for the IF combined code and carrier phase observations, respectively.

The IF combined observations are often used to estimate the precise satellite clocks for the analysis centers. The IF combined UCDs at the satellite will be fully assimilated into the estimates of satellite clock offsets, but they can be eliminated when applying the precise clock products to the observations of the same frequency in the PPP processing. The satellite clock estimates read:

$$c\mathrm{d}t^s_{IF} = c\mathrm{d}t^s + b^s_{IF} + dD^{AC} \tag{2}$$

where dD^{AC} denotes the clock offset reference introduced by the respective analysis center for PCE. After applying the precise satellite orbit and clock products, and correcting the tropospheric dry delay with a priori model, Equation (1) can be rewritten as follows:

$$\begin{cases} p_{IF} = \boldsymbol{\mu} \cdot \mathbf{X} + c\bar{\mathrm{d}}t_r + m \cdot Z_w \\ l_{IF} = \boldsymbol{\mu} \cdot \mathbf{X} + c\bar{\mathrm{d}}t_r + m \cdot Z_w + \lambda_{IF} \cdot \bar{N}_{IF} \end{cases} \tag{3}$$

with

$$\begin{cases} c\bar{\mathrm{d}}t_r = c\mathrm{d}t_r + b_{r,IF} + dD^{AC} \\ \bar{N}_{IF} = N_{IF} + d_{r,IF} - d^s_{IF} \\ d_{r,IF} = B_{r,IF} - b_{r,IF}/\lambda_{IF} \\ d^s_{IF} = B^s_{IF} - b^s_{IF}/\lambda_{IF} \end{cases} \tag{4}$$

where p_{IF} and l_{IF} are the code and phase observed-minus-computed (OMC) observables, respectively, $\boldsymbol{\mu}$ denotes the unit vector of line of sight direction, $\mathbf{X}$ denotes the vector of receiver coordinates in the three dimensions, m is the elevation-dependent wet mapping function, and Z_w denotes the tropospheric zenith wet delay (ZWD).

Although the QZSS and GPS signals adopt the same center frequency and the system time difference is very small, the receivers receive and process satellite signals using different receiving and processing units for GPS and QZSS. Therefore, an ISB parameter still needs to be introduced into GPS and QZSS combined data processing. The observation model of GPS/QZSS integrated PPP can be established as follows:

$$\begin{cases} p^G_{IF} = \boldsymbol{\mu}^G \cdot \mathbf{X} + c\bar{\mathrm{d}}t_{r,G} + m^G \cdot Z_w \\ l^G_{IF} = \boldsymbol{\mu}^G \cdot \mathbf{X} + c\bar{\mathrm{d}}t_{r,G} + m^G \cdot Z_w + \lambda^G_{IF} \cdot \bar{N}^G_{IF} \\ p^J_{IF} = \boldsymbol{\mu}^J \cdot \mathbf{X} + c\bar{\mathrm{d}}t_{r,G} + ISB^{G,J} + m^J \cdot Z_w \\ l^J_{IF} = \boldsymbol{\mu}^J \cdot \mathbf{X} + c\bar{\mathrm{d}}t_{r,G} + ISB^{G,J} + m^J \cdot Z_w + \lambda^J_{IF} \cdot \bar{N}^J_{IF} \end{cases} \tag{5}$$

with

$$ISB^{G,J} = (b^J_{r,IF} - b^G_{r,IF}) + (dD^{J,AC} - dD^{G,AC}) \tag{6}$$

where the superscripts G and J refer to GPS and QZSS, respectively, $(b^J_{r,IF} - b^G_{r,IF})$ is the difference of the receiver-dependent code hardware delay between QZSS and GPS, and $(dD^{J,AC} - dD^{G,AC})$ is caused by the different clock datum constraints of QZSS and GPS employed by the analysis center. It can be concluded that the ISB not only depends on the receiver-specific code hardware delays but also relies on the satellite clock datum used by the analysis center when estimating the precise satellite clocks.

III. DYNAMIC MODELS FOR ISB PARAMETER

In addition to the necessary observation model, the dynamic model of the state vectors also strongly influences the optimality of the parameters in Kalman filter. The dynamic noises of the state vectors describe the effect of their relative uncertainty on the motion state. The random walk process, constant and white noise process can be used to describe the dynamic noises of ISB parameter.

The random walk model means that the parameter has a high time correlation, but the small variations over time are also considered. Usually, the tropospheric ZWD parameter can be described as random walk process in PPP. The random walk process for the ISB parameter can be described as:

$$ISB(k) = ISB(k-1) + \tau_v,\ \tau_v \sim N(0, \sigma^2_{\tau_v}) \tag{7}$$

where k represents the epoch number, τ_v can be considered as the time-varying part of ISB, which follows the Gaussian distribution, and $\sigma^2_{\tau_v}$ denotes the variance of the ISB dynamic noises.

The constant model implies that the parameter is very stable and will not change over time. Actually, the constant model is a special case of the random walk model, provided that τ_v is zero. The static receiver coordinates and the phase ambiguity parameters can be expressed as constants in PPP. The ISB parameter can be modeled as constants, that is:

$$ISB(k) = ISB(k-1) \tag{8}$$

The white noise model shows that the parameter is independent among different epochs. The kinematic receiver

coordinates, the receiver clocks and the ionospheric delay parameters are usually estimated as white noise process in PPP. The white noise estimation for the ISB parameter can be expressed as:

$$ISB(k) \sim N(ISB_0(k), \sigma^2_{ISB}) \tag{9}$$

where ISB_0 represents the initial value of ISB, and σ^2_{ISB} represents the initial a priori variance of ISB.

IV. DATA DESCRIPTION AND PROCESSING STRATEGY

In order to investigate the current positioning performance of standalone QZSS PPP, the datasets from a total of 11 MGEX tracking stations located in the QZSS service area spanning 11 consecutive days from 5 to 15 December 2019 are selected. The geographical distribution of the stations is shown in Figure 1. All the selected stations are within the ground tracks of QZSS satellites, and therefore they can track all the four QZSS satellites simultaneously for a long time. The selected stations are all equipped with the geodetic-type receivers, and the detailed equipment information is shown in Table 1. Among all the MGEX analysis centers, GFZ, WUM and TUM can provide the precise products for all the four QZSS satellites. However, the QZSS precise products provided by TUM are often absent, and the TUM products are not updated during the analysis period. Thus, only the precise products from GFZ and WUM are used to calculate the satellite coordinates and the satellite clock offsets. The sampling intervals of GFZ orbit and clock offset products are 5 min and 30 s, respectively, and those of WUM orbit and clock offset products are 15 min and 30 s, respectively. The precision of the GPS code and phase observations is set to 0.3 and 0.003 m, respectively. Since the current precise products of QZSS are not as good as those of GPS, the weight ratio between QZSS and GPS observations is set to 1:4. The "igs14.atx" file provided by IGS is used to correct the satellite phase center offsets (PCOs) and the satellite phase center variations (PCVs). Currently, the PCV corrections of the first QZSS satellite (J01) are still unavailable. The PCO and PCV corrections of the receiver antenna on QZSS L1 and L2 frequencies are simply replaced by those on GPS L1 and L2 frequencies, respectively. The detailed processing strategies are shown in Table 2. Both static and kinematic positioning modes are employed, and the SINEX file provided by IGS is used as the reference of station coordinates to evaluate the positioning accuracy. In GPS/QZSS combined PPP, four different processing strategies are adopted for the ISB parameter, namely ignoring the ISB (ISB-IN), estimated as constants (ISB-CT), estimated as random walk process (ISB-RW) and estimated as white noise process (ISB-WN). The open source program package RTKLIB is used for the data processing in this paper [19], but we have made improvements in many aspects, such as the proper consideration of ISB in GPS/QZSS integrated PPP.

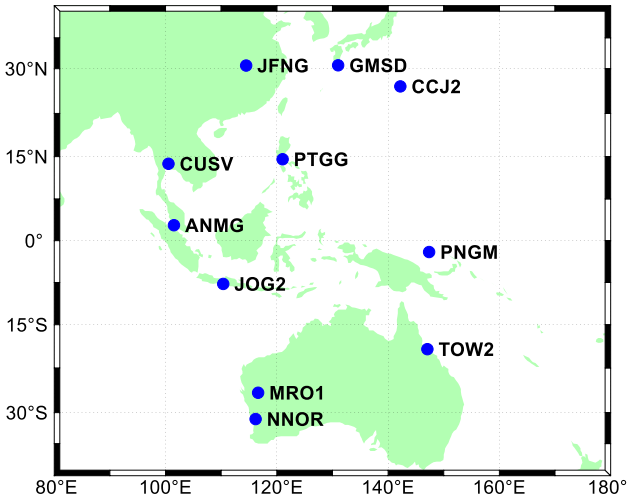

FIGURE 1. Geographical distribution of the 11 adopted MGEX tracking stations.

V. RESULTS AND ANALYSIS

In this section, we first analyze the phase multipath and noise (PMN) as well as the phase-specific inter-frequency clock bias (PIFCB). Subsequently, the positioning accuracy and convergence time of QZSS-only PPP are assessed, and the obtained results are also compared with those of GPS-only PPP. Next, we rigorously study the effects of the four different ISB processing strategies (ignoring ISB as well as estimating ISB as constant, random walk process and white noise process) on the QZSS/GPS positioning results. Also, the ISB estimates derived from the QZSS/GPS PPP are characterized. Then, we discuss the enhancement of QZSS observations to the GPS precise positioning in the harsh visibility environment, which is also the original intention for the design of QZSS. Finally, the post-processed kinematic position solutions as well as the real-time static and kinematic position solutions with L6E orbit and clock corrections are described.

A. PIFCB AND PMN

Actually, besides the stable code hardware delay, the satellite clock offset parameters will also absorb the time-varying phase hardware delay when performing the PCE [20]. Therefore, there are differences, termed inter-frequency clock bias (IFCB), in the estimated satellite clock products using two different IF combinations (such as L1/L2 and L1/L5), since the hardware delay is related to the frequency. The IFCB can be divided into the code-specific IFCB (CIFCB) and the phase-specific IFCB (i.e., PIFCB). Due to the conversion between CIFCB and differential code biases (DCBs) and the much greater weights of phase observations than code observations, many scholars are more concerned about the PIFCB. For fast PIFCB estimation, the differenced IF (DIF) phase observations between L1/L2 and L1/L5 dual-frequency IF combinations are composed, and then the constant phase ambiguity and the stable part of phase hardware delay can be eliminated by removing the mean value of DIF time series

TABLE 1. Receiver types, antenna types, firmware versions and station locations of the 11 adopted stations.

Station	Latitude (°)	Longitude (°)	Receiver Type	Antenna Type		Firmware Version
ANMG	2.78	101.51	TRIMBLE NETR9	JAVRINGANT_DM	SCIS	5.37
CCJ2	27.07	142.20	TRIMBLE NETR9	TRM59800.00	SCIS	5.37
GMSD	30.56	131.02	TRIMBLE NETR9	TRM59800.00	SCIS	5.37
MRO1	-26.70	116.64	TRIMBLE NETR9	TRM59800.00	NONE	5.37
PNGM	-2.04	147.37	TRIMBLE NETR9	TRM59800.00	NONE	5.37
JFNG	30.52	114.49	TRIMBLE NETR9	TRM59800.00	NONE	5.42
PTGG	14.54	121.04	SEPT POLARX5	TRM59800.00	SCIS	5.3.0
TOW2	-19.27	147.06	SEPT POLARX5	LEIAR25.R3	NONE	5.2.0
NNOR	-31.05	116.19	SEPT POLARX5TR	SEPCHOKE_B3E6	NONE	5.3.0
JOG2	-7.76	110.37	JAVAD TRE_G3TH DELTA	JAV_RINGANT_G3T	NONE	3.7.5p1
CUSV	13.74	100.53	JAVAD TRE_3 DELTA	JAVRINGANT_DM	NONE	3.7.6

TABLE 2. Processing strategies for the PPP.

Items	Strategies
Observations	Pseudo-range and carrier phase observations
Signal selection	GPS: L1/L2, QZSS: L1/L2
Sampling rate	30 s
Cut-off elevations	7° or 30°
Weighting scheme	Elevation-dependent weight
Estimator	Kalman filter
Satellite orbits and clocks	Fixed with the products from MGEX in the post-processed scenario, and with the broadcast ephemeris and L6E corrections in the real-time scenario
Phase wind-up effect	IERS conventions 2010
Earth rotation parameters	Fixed
Relativistic effect	IERS conventions 2010
Station displacement	Solid Earth tide, Ocean tide, Pole tide, IERS conventions 2010
Phase center offset	Satellite: corrected using IGS values Receiver: corrected using GPS values from IGS
Phase center variation	Satellite: corrected using IGS values, except for J01 Receiver: corrected using GPS values from IGS
Ionospheric delay	First-order effect eliminated by IF linear combination
Tropospheric dry delay	Corrected using Saastamoinen model
Tropospheric wet delay	Estimated as random walk process
Station coordinates	Estimated as constants in static mode, and as white noise process in kinematic mode
Receiver clock	Estimated as white noise process
ISB	ISB-IN: Ignored ISB-CT: Estimated as constants ISB-RW: Estimated as random walk process ISB-WN: Estimated as white noise process
Phase ambiguities	Estimated as float constants

in each continuous ambiguity arc [21]. The single-station PIFCB estimation is not highly reliable and accurate, but the derived estimates can still be used to analyze the time-varying characteristics of PIFCB.

The epoch-wise PIFCB time series of QZSS and GPS at GMSD and MRO1 stations on 5 December 2019 are shown in Figure 2. The two stations are capable of receiving the triple-frequency signals (L1, L2 and L5) of GPS and QZSS. The PIFCB results from the 12 GPS Block IIF satellites (G01/G03/G06/G08/G09/G10/G24/G25/G26/G27/G30/G32) and all the four QZSS satellites are compared. It can be clearly seen that the PIFCB time series of the GPS satellites change over time with an amplitude of up to 0.1 m. For the QZSS satellites, no obvious bias can be observed and the PIFCB behaves more like the noises in comparison with GPS satellites. It is indicated that the PIFCB of the QZSS satellites can be ignored. The fluctuation of the PIFCB time series of QZSS satellites is mainly affected by the phase multipath and noise (i.e., PMN).

Based on the previously obtained PIFCB time series, the epoch-difference strategy is used to remove the long-term trends, and the residuals mainly contain the PMN. As such, the PMN of QZSS and GPS satellites can be calculated. The relationship between the RMSs of the epoch-wise PMN values and the satellite elevation angles using the datasets over the whole analysis period (11 days from 5 to 15 December 2019) at GMSD and MRO1 stations is shown in Figure 3. The PMN RMS value is calculated with an interval of 5° in terms of the satellite elevations. The elevation of the J07 (GEO satellite) is basically unchanged, so a five-pointed star at a respective elevation of 52.5° and 57.5° for GMSD and MRO1 stations is used to identify the PMN values of this satellite. Similarly, 12 GPS Block IIF satellites and four QZSS satellites are selected. It can be seen that the changes of GPS and QZSS PMN values with elevation angles are very similar, and the PMN values reduce from approximately 10 to 2 mm with increasing elevations from about 10° to nearly zenith. The results indicate that the precision of QZSS phase observations is comparable to that of GPS ones.

B. PERFORMANCE OF QZSS-ONLY PPP

This section investigates the performance of QZSS-only PPP in a static mode, and also conducts a performance comparison with GPS-only PPP. Figure 4 exhibits the epoch-wise RMSs of position errors in the east, north and up directions for QZSS-only and GPS-only PPP using GFZ and WUM precise products. The epoch-wise RMSs are calculated using the positioning errors at the common epoch (with the same time

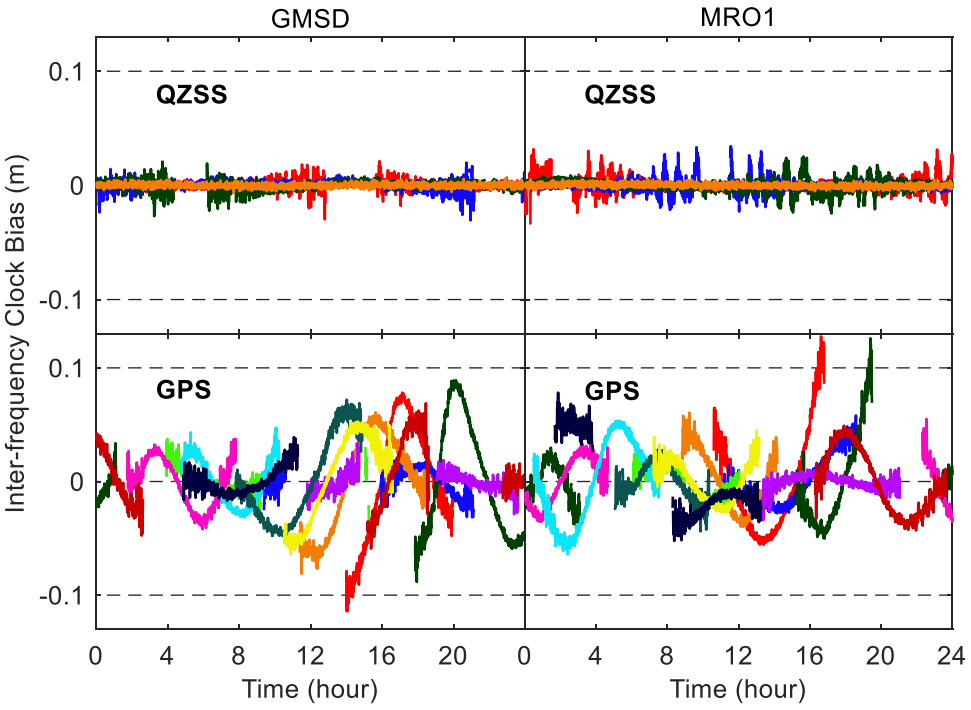

FIGURE 2. Epoch-wise PIFCB time series of QZSS and GPS Block IIF satellites at GMSD and MRO1 stations on 5 December 2019.

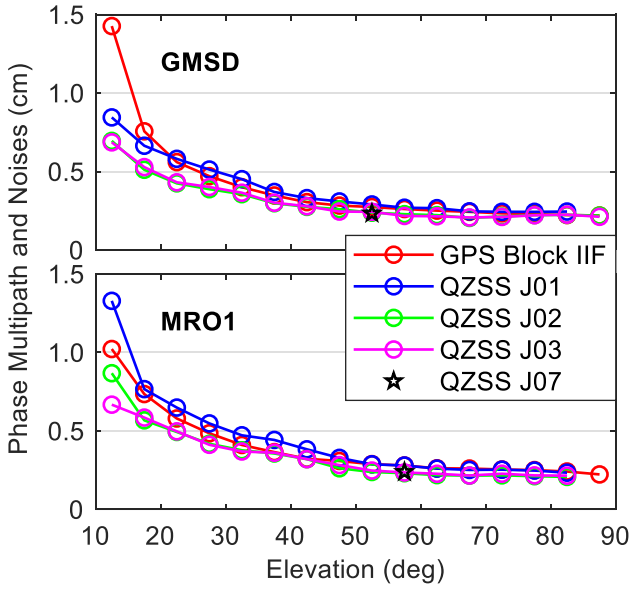

FIGURE 3. Dependence of PMN values on satellite elevations for QZSS and GPS Block IIF satellites at GMSD and MRO1 stations based on the datasets spanning 11 days.

span from the first epoch) of all stations (11 stations) from all the days (11 days). For example, the position errors at the epoch with a time span of four hours from the first epoch (for each session) over all the 121 daily solution files are used to compute the epoch-wise RMSs at the epoch 4:00. Since few stations are able to track all the four QZSS satellites for 24 consecutive hours, Figure 4 only shows the GPS-only and QZSS-only PPP results in the first 20 hours. It can be seen that the positioning accuracy of QZSS-only PPP with four available satellites is approximately 4, 2 and 15 cm after the position filter converges to stable values in the three directions, respectively. As for the GPS-only PPP, the corresponding positioning accuracy is usually better than 2, 1 and 2 cm in the three directions, respectively. Table 3 provides the numerical value for the epoch-wise RMSs of position errors at the epoch undergoing a processing time of 20 hours. Using GFZ products, the fully converged positioning accuracy of QZSS-only PPP is 2.8, 1.6 and 14.5 cm in the three directions, respectively. The corresponding statistics are 3.5, 1.6 and 16.1 cm when adopting the WUM products in the three directions, respectively, which are slightly worse than those with GFZ products. For GPS-only PPP, the positioning results using GFZ and WUM products are in good agreement, and the difference is less than 0.2 cm in terms of the position accuracy statistics. Using GFZ products, the fully converged positioning accuracy of GPS-only PPP is 1.0, 0.3 and 1.2 cm in the three directions, respectively.

TABLE 3. Epoch-wise RMSs of position errors at the epoch undergoing a processing time of 20 hours for QZSS-only and GPS-only PPP with different precise products based on the datasets from 11 stations spanning 11 days.

Products	Direction	QZSS	GPS
GFZ	East (cm)	2.8	1.0
	North (cm)	1.6	0.3
	Up (cm)	14.5	1.2
WUM	East (cm)	3.5	0.9
	North (cm)	1.6	0.3
	Up (cm)	16.1	1.4

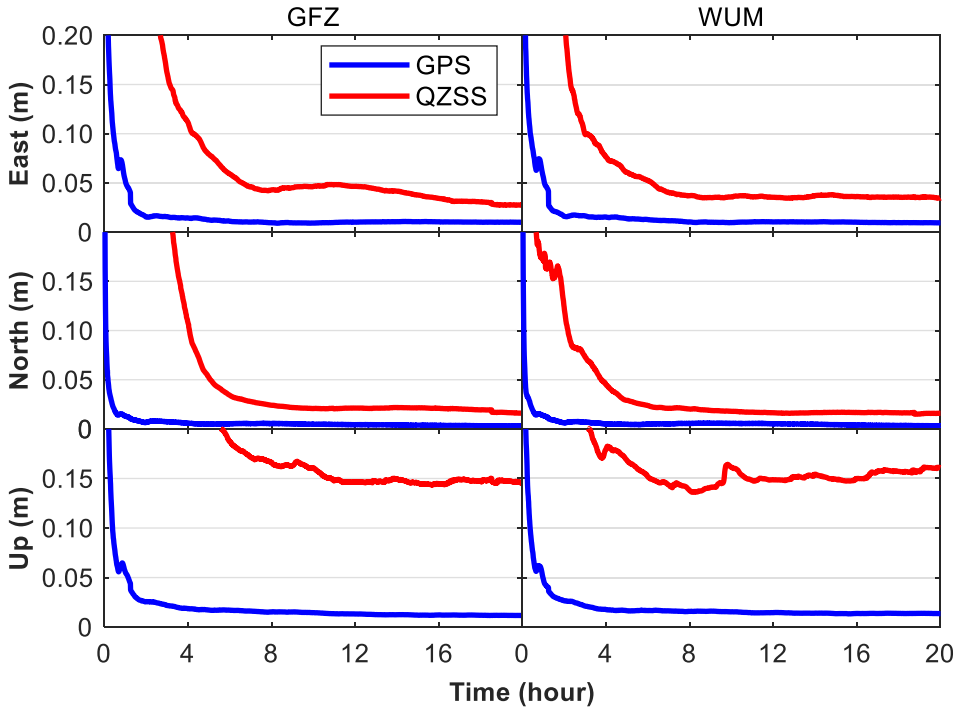

FIGURE 4. Epoch-wise RMSs of position errors for QZSS-only and GPS-only PPP using GFZ and WUM precise products based on the datasets from 11 stations spanning 11 days.

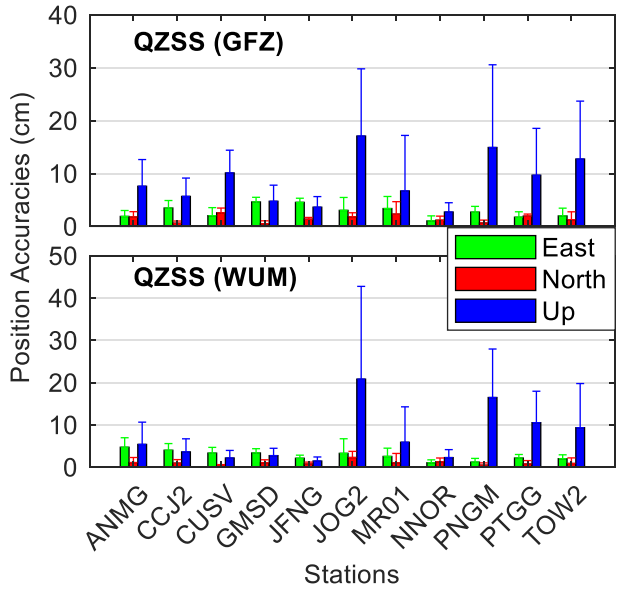

FIGURE 5. Station-specific average positioning accuracy at the epoch undergoing a processing time of 20 hours over 11 days as well as the corresponding STD statistics for each station for QZSS-only PPP.

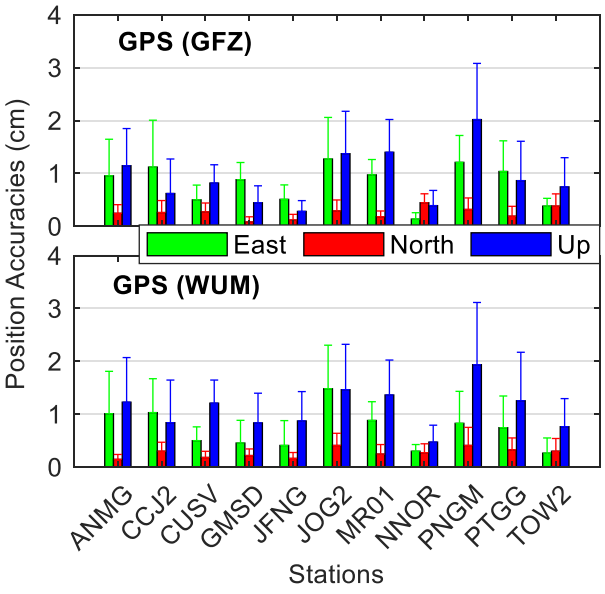

FIGURE 6. Station-specific average positioning accuracy at the epoch undergoing a processing time of 20 hours over 11 days as well as the corresponding STD statistics for each station for GPS-only PPP.

For further analysis, Figures 5 and 6 provide the station-specific average positioning accuracy over 11 days for each station for QZSS-only and GPS-only PPP, respectively. The absolute value of the position error at the epoch undergoing a processing time of 20 hours is taken as the fully converged positioning accuracy for each session. In addition, the short horizontal lines above the bars in Figures 5 and 6 refer to the STD statistics of the single-day positioning accuracy over 11 days for each station. For GPS-only PPP, due to the sufficient number of visible satellites, the difference of average positioning accuracy among the 11 stations is not obvious, and the day-to-day scattering (i.e., STD statistics)

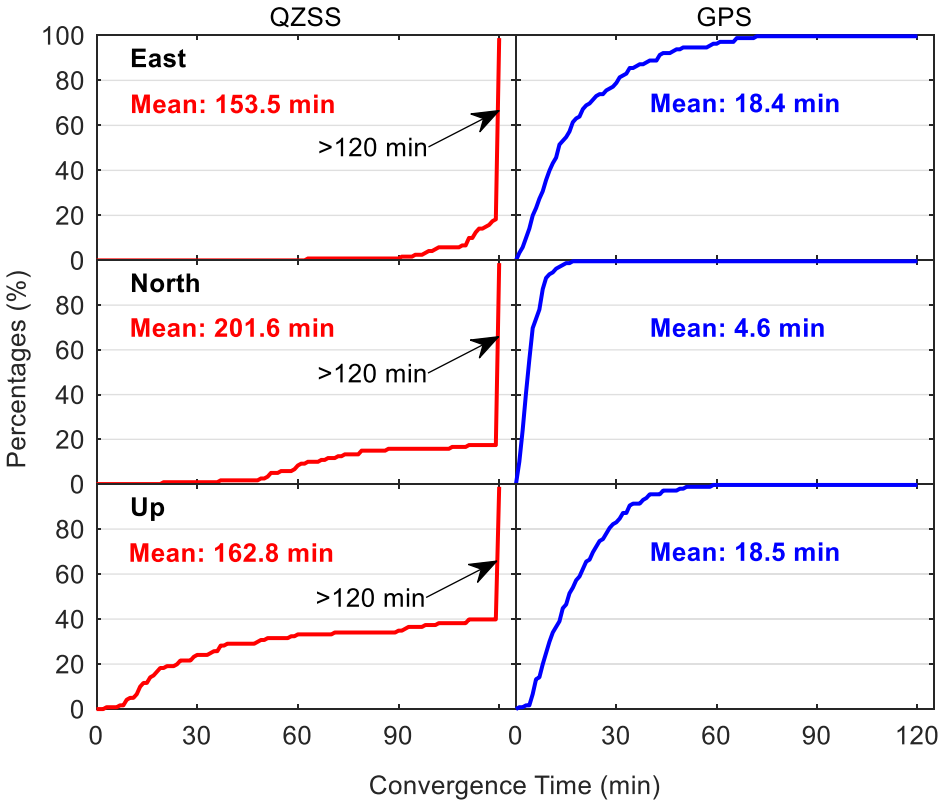

FIGURE 7. A linear statistic of cumulative distribution of convergence time for QZSS-only and GPS-only PPP using GFZ final products based on the datasets from 11 stations spanning 11 days.

of the single-day positioning accuracy over the 11 days is usually smaller than 1 cm. By contrast, the average positioning accuracy of the QZSS-only PPP with only four available satellites shows significant differences among the 11 stations, especially for the up direction, and the vertical accuracy difference can be as large as 14.4 and 19.4 cm using the GFZ and WUM products, respectively. Regarding the day-to-day scattering of single-day positioning accuracy in the up direction for the QZSS-only PPP solutions, it can reach 15.6 cm using GFZ products at station PNGM, and 21.9 cm using WUM products at station JOG2, respectively.

A linear statistic of cumulative distribution of convergence time for GPS-only and QZSS-only PPP using GFZ and WUM products is depicted in Figures 7 and 8, respectively. The determination of convergence for the position solutions at a specific epoch is that the positioning errors are smaller than 0.1 m for the next ten continuous epochs. It should be noted that, due to the poor positioning performance of the QZSS-only PPP in the up direction, the corresponding convergence threshold is enlarged to 0.2 m. It is important to notice that the initialization time, namely time-to-first-fix (TTFF), is an important index to reflect the efficiency of achieving an ambiguity-fixed solution, but it is not covered here as this paper only focuses on the ambiguity-float solutions. Figures 7 and 8 also show the average convergence time for all the employed stations and days, and the cases with a convergence time longer than 120 min are indicated by the numerical values at the 120 min in the two figures. It is worth noting that the average convergence time of QZSS-only PPP using GFZ products exceeds 120 min in all three directions, while that of using WUM products is significantly better, which is 75.2, 44.3 and 45.6 min in the east, north and up coordinate directions, respectively. When employing the WUM products, the QZSS-only PPP solutions with a convergence time shorter than 60 min account for 49%, 79% and 78% in the three directions, respectively. For GPS-only PPP, the convergence performance using WUM products is slightly better than that using GFZ products, and the difference of average convergence time between them is within 3 min. The average convergence time of GPS-only PPP with WUM products is 16.0, 4.0 and 17.1 min in the three directions, respectively. For further analysis, a comprehensive convergence threshold is determined to analyze the convergence time of the comprehensive direction (i.e., the 3D convergence time). When the position errors in all the three directions simultaneously keep within 0.1 m for ten continuous epochs, the 3D position filter is considered to converge. In view that the vertical positioning performance of QZSS-only PPP is poor, its convergence of the 3D position filter at a specific epoch is determined, provided that the position errors in the east, north and up directions simultaneously keep within 0.1, 0.1 and 0.2 m for the next ten continuous epochs (including

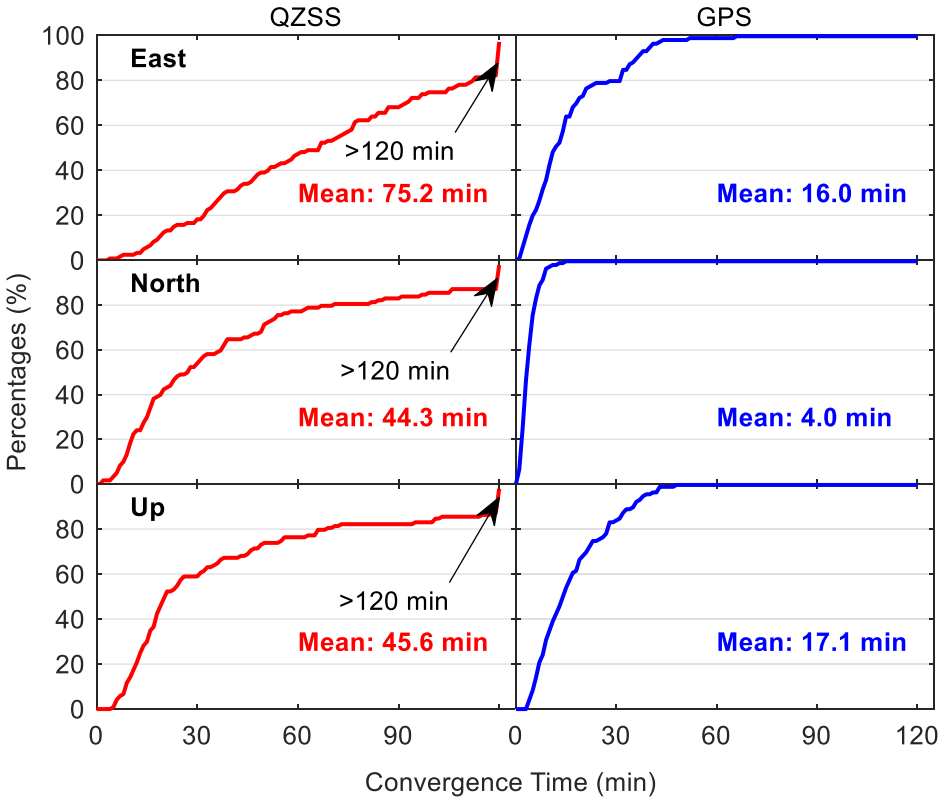

FIGURE 8. A linear statistic of cumulative distribution of convergence time for QZSS-only and GPS-only PPP using WUM final products based on the datasets from 11 stations spanning 11 days.

this epoch), respectively. The average 3D convergence time for QZSS-only and GPS-only PPP using GFZ products is 246.8 and 23.5 min, respectively, while the corresponding 3D convergence time using WUM products decreases to 94.3 and 21.3 min, respectively. A comparative analysis of the results shown in Figures 7 and 8 indicates that the QZSS-only PPP obtains worse position solutions when using GFZ products. Following Li *et al.* [7], the along-track difference between the precise satellite orbit corrections from WUM and GFZ could reach several meters for the GEO satellite J07. Thus, the generation strategy of GFZ precise products for QZSS satellites may need to be improved.

C. PERFORMANCE OF GPS/QZSS COMBINED PPP

This section first studies which estimation strategy (dynamic model) should be adopted for the ISB parameter in GPS and QZSS integrated PPP. A static mode is employed in this section. Figure 9 depicts the time series of epoch-wise RMSs of position errors for GPS/QZSS PPP under different ISB estimation strategies with GFZ and WUM products. ISB-IN represents ignoring the ISB between QZSS and GPS, while ISB-CT, ISB-RW and ISB-WN denote estimating the ISB as constant, random walk process and white noise process, respectively. Table 4 lists the average epoch-wise RMSs for the last half hour. When using GFZ products, the positioning results of ISB-IN and ISB-CT cases in the east and up directions are very poor, which are even much worse than those of GPS-only PPP (see Figure 4 and Table 3). As for ISB-RW and ISB-WN cases with GFZ products, they have similar positioning performance, and the average positioning accuracy over the last half hour is 0.5, 0.3 and 1.3 cm in the east, north and up components, respectively. With the use of WUM products, the positioning performance is comparable for the four cases employing different ISB processing strategies, the position accuracy of which is 0.4 and 0.2 cm in the east and north directions, and 1.0 cm for the ISB-IN case and 1.3 cm for the other three cases in the up direction, respectively. The derived ISB estimates using WUM products for the ISB-CT, ISB-RW and ISB-WN cases are consistent with each other, and all show stable characteristics (see Figure 12). Thus, when employing WUM products, the positioning accuracy of GPS/QZSS combined PPP is at a similar level for the three different ISB handling strategies. As for the ISB-IN case, the phase ambiguity parameters can absorb the stable hardware delays, and only the code observations will be affected by the inconsistent receiver-dependent code hardware delays between GPS and QZSS. In view that the magnitude of ISBs using WUM products is relatively small (see Figure 12), and the code observations have much smaller weights than the phase observations, the effects of the inconsistent code hardware delays on the GPS/QZSS PPP solutions are very limited. By contrast, when using GFZ products, the larger magnitude of ISBs and the time-varying characteristics of ISBs (see Figure 12) result in distinct GPS/QZSS PPP solutions.

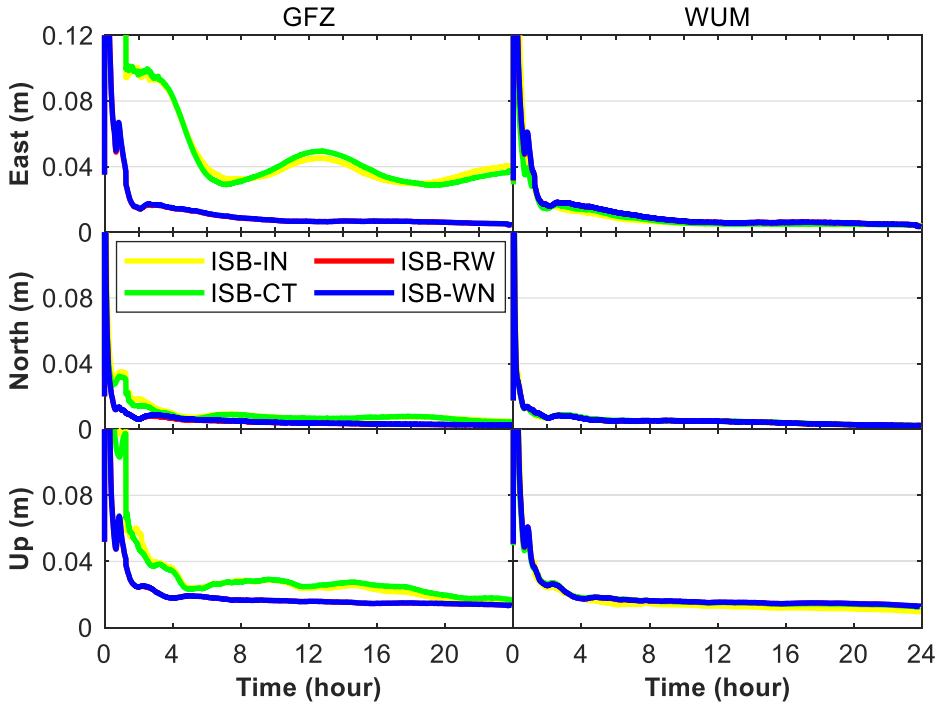

FIGURE 9. Epoch-wise RMSs of position errors for GPS/QZSS PPP with different ISB handling strategies using GFZ and WUM products based on the datasets from 11 stations spanning 11 days.

TABLE 4. Average values of epoch-wise RMSs of position errors over the last half hour for GPS/QZSS PPP with different ISB handling strategies using GFZ and WUM products based on the datasets from 11 stations spanning 11 days.

Products	Item	ISB-IN	ISB-CT	ISB-RW	ISB-WN
GFZ	East (cm)	4.0	3.7	0.5	0.5
	North (cm)	0.5	0.5	0.3	0.3
	Up (cm)	1.7	1.7	1.3	1.3
WUM	East (cm)	0.4	0.4	0.4	0.4
	North (cm)	0.2	0.2	0.2	0.2
	Up (cm)	1.0	1.3	1.3	1.3

Figure 10 shows the convergence time of GPS/QZSS PPP with different ISB estimation strategies when using GFZ products. The convergence criterion is that the positioning error is smaller than 0.1 m and continuously maintains this for the next ten epochs. It can be seen that for using GFZ products, similar convergence performance can be achieved when ISB is estimated as random walk and white noise processes. The average results over all the 24-hour sessions are presented in each panel. The average convergence time is about 15 min in the east and up directions, and 5 min in the north direction for both ISB-RW and ISB-WN cases, respectively. Compared with these results, ignoring the ISB or estimating the ISB as constants will significantly prolong the convergence time, especially for the east and up directions. The position results with convergence time longer than 60 minutes account for approximately 15%–30% in the east and up directions. It is worth pointing out that the positioning and convergence performance in these two cases are much worse than those of GPS-only PPP, which is unreasonable in the multi-system integrated positioning. As for the average 3D convergence time, the statistical value is 93.2, 80.4, 20.0 and 19.6 min for ISB-IN, ISB-CT, ISB-RW and ISB-WN cases, respectively.

Figure 11 shows the corresponding results of convergence time using WUM products, which are far different from those using GFZ products. Except for the ISB-IN case in the east direction, the convergence performance under the four ISB estimation strategies is comparable for the GPS/QZSS PPP. The average convergence time is about 14, 4 and 15 min for ISB-RW and ISB-WN cases in the east, north and up directions, respectively, which is slightly worse than that for ISB-CT case with an average statistic of 11.5, 3.8 and 14.2 min in the three directions, respectively. It is worth pointing out that in terms of ISB estimation strategies, regardless of using GFZ or WUM products, the worst convergence performance can be achieved when ignoring ISB. This also demonstrates that the ISB between GPS and QZSS must be considered in the integrated processing. The average 3D convergence time is 24.4, 16.6, 18.5 and 18.9 min for ISB-IN, ISB-CT, ISB-RW and ISB-WN cases, respectively.

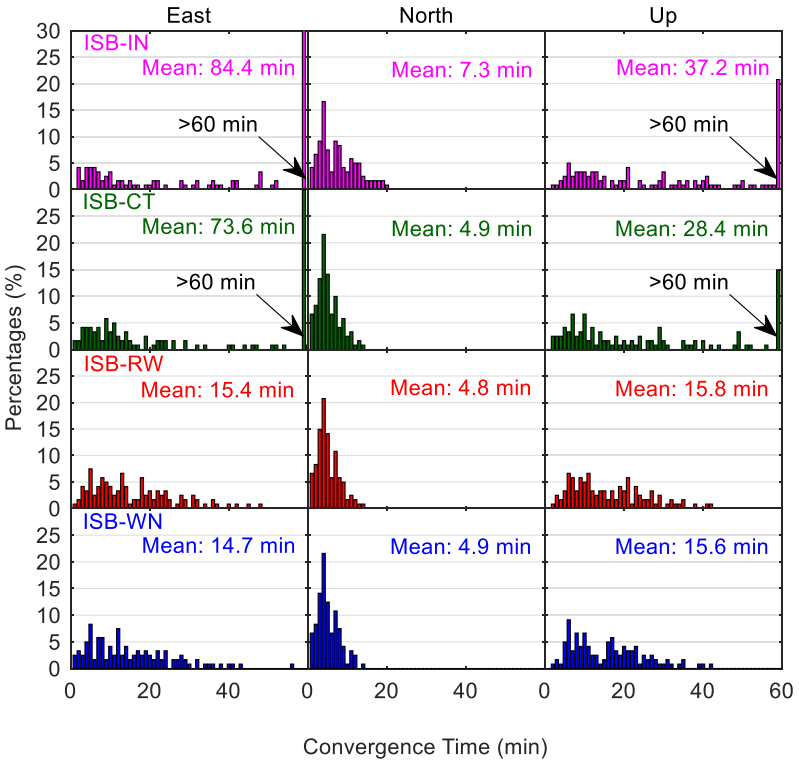

FIGURE 10. Distribution of convergence time for GPS/QZSS PPP with different ISB handling strategies using GFZ final products based on the datasets from 11 stations spanning 11 days.

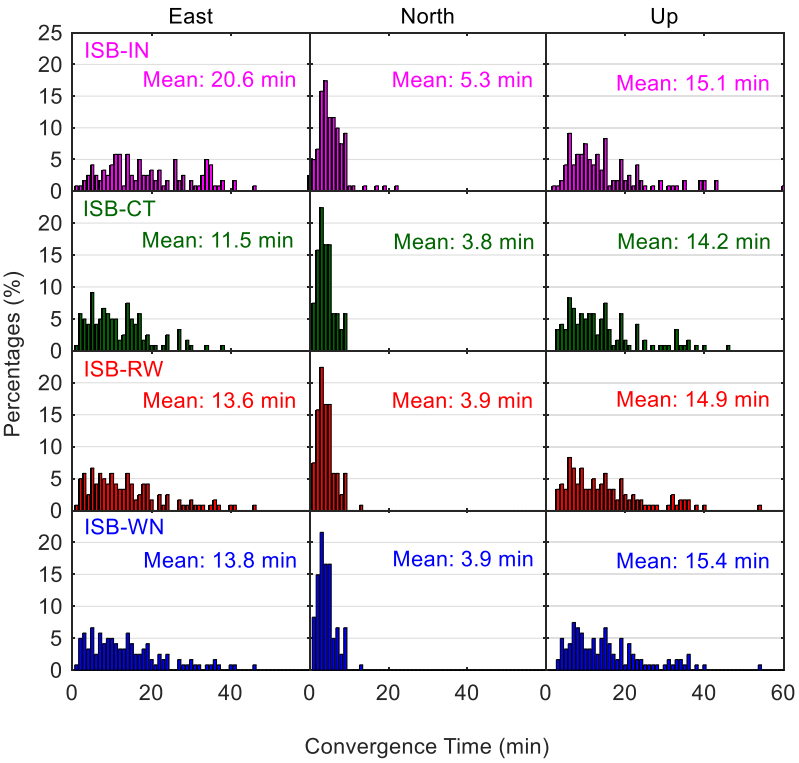

FIGURE 11. Distribution of convergence time for GPS/QZSS PPP with different ISB handling strategies using WUM final products based on the datasets from 11 stations spanning 11 days.

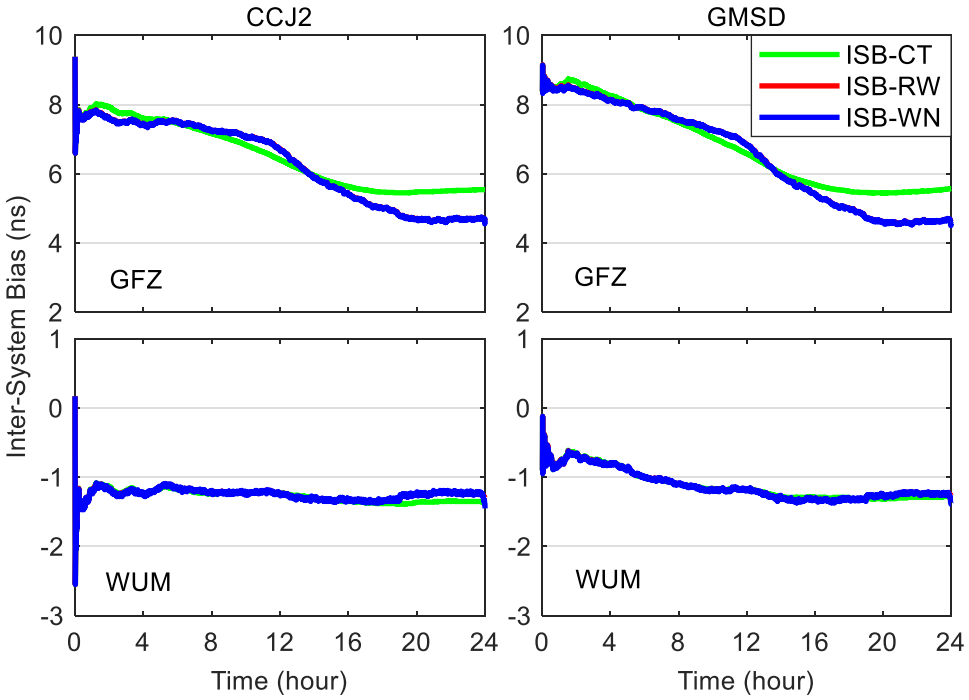

FIGURE 12. Epoch-wise ISB estimates under different ISB handling strategies using GFZ and WUM final products at CCJ2 and GMSD stations on 10 December 2019.

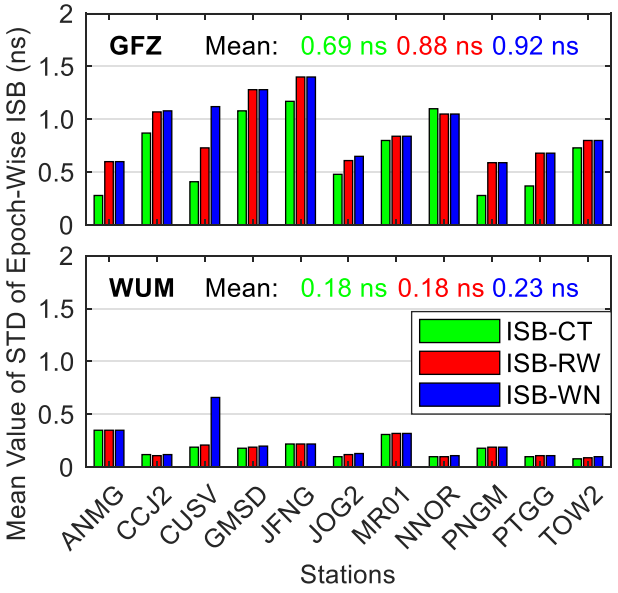

FIGURE 13. Average values of STDs of epoch-wise ISB over a day for 11 days under different ISB handling strategies using GFZ and WUM final products at 11 MGEX stations.

The characteristics of ISB estimates derived from GPS/QZSS combined PPP with different dynamic models for ISB parameters (i.e., ISB-CT, ISB-RW and ISB-WN) are analyzed in this section. The time series of 1-day epoch-wise ISB estimates under three different ISB estimating strategies at CCJ2 and GMSD stations on 10 December 2019 are plotted in Figure 12. The selected two stations are both equipped with TRIMBLE NETR9 receiver and TRM59800.00 SCIS antenna with the firmware version 5.37, so as to mitigate the receiver-specific influence on ISB estimation. It can be seen that the estimated ISB using GFZ products is not stable enough, and shows a curve with a varying range of more than 2.0 ns. The estimated ISB with the ISB-RW strategy is comparable to that with the ISB-WN strategy, in view of an overlap of the red and blue curves. By contrast, the estimated ISBs using WUM products under the three different dynamic models are all stable and the differences among them are less than 0.1 ns for most of the cases. To investigate the short-term stability of ISB estimates, the STD values of epoch-wise ISB over a day are computed for each station and each day. Figure 13 provides the average results of the derived single-day STD values over the whole analysis period (11 days) for each station. As the same as the conclusion derived from Figure 12, the short-term stability of ISB estimated by the WUM products is higher than that of the GFZ products. The average STD values of single-day epoch-wise ISB over all the days and stations of the ISB-CT, ISB-RW and ISB-WN cases are 0.69, 0.88 and 0.92 ns for the GPS/QZSS PPP with GFZ products, and 0.18, 0.18 and 0.23 ns for the GPS/QZSS PPP with WUM products, respectively.

For the purpose of investigating the long-term stability of ISB, Figure 14 plots the time series of the 11-day daily ISB (i.e., average value of the 1-day epoch-wise ISB). In Figure 14, different colors are used to identify different receiver types. Due to the instability of the epoch-wise ISB during the convergence period, the time series in the first one hour are excluded when calculating the daily ISB values.

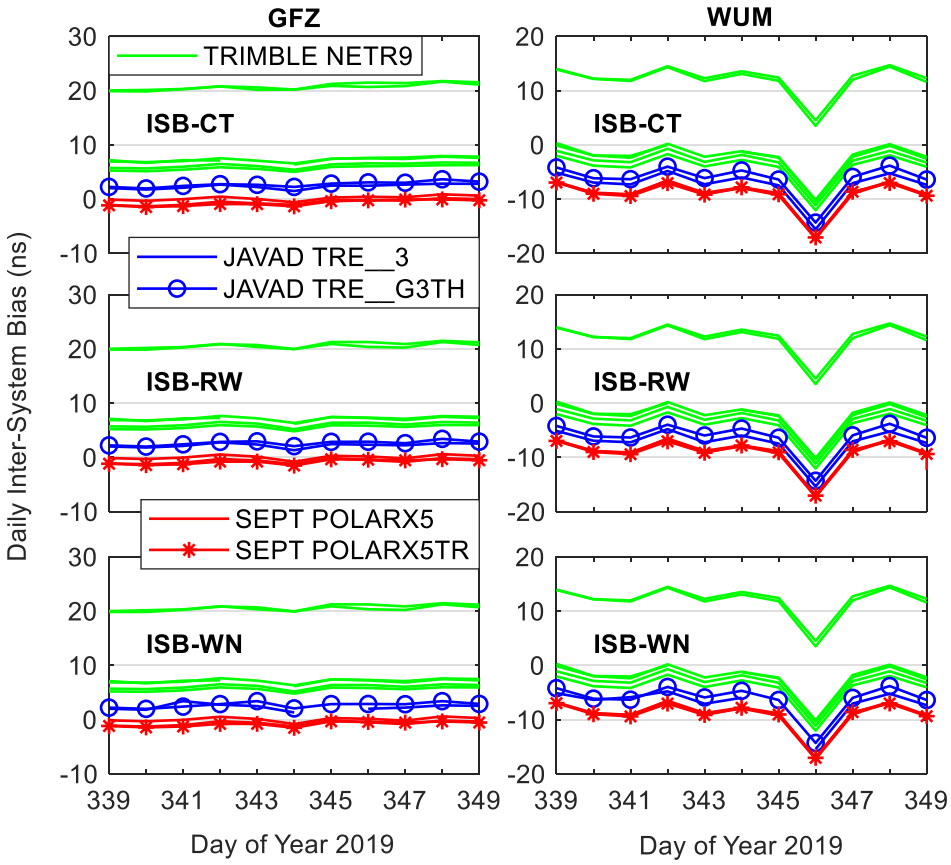

FIGURE 14. Daily ISB characterized by the receiver types under different ISB handling strategies using GFZ and WUM final products.

On the day of year (DOY) 346 of 2019 (i.e., 12 December 2019), the estimated ISB using WUM products produces a large jump at all stations. The common jump of daily ISB can be attributed to the employed precise products, and the abnormal jump is ruled out in the next analysis. It is noted that the daily ISB is roughly consistent for the stations equipped with the same type of receivers, except for the PNGM and MRO1 stations with TRIMBLE NETR9 receiver. The STD values of daily ISB over 11 days are calculated for each station, and the obtained results are given in Figure 15. The average results over all the stations are also provided in the figure. It is worth noting that the long-term stability of ISB between QZSS and GPS estimated with GFZ products is better than that of WUM products. For using GFZ products, the average STD values of daily ISB under the ISB-CT, ISB-RW and ISB-WN strategies are 0.49, 0.43 and 0.45 ns, respectively. For using WUM products, the corresponding statistics are increased to 1.06, 1.06 and 1.05 ns, respectively.

QZSS was originally designed to improve the positioning performance of GPS under high elevation angles. In order to explore the enhanced performance that benefits from QZSS in harsh environments, we analyze the positioning performance of GPS/QZSS PPP at the cut-off elevation of 30°. Based on the previous analysis, the ISB between GPS and QZSS is recommended to be estimated as constants when using

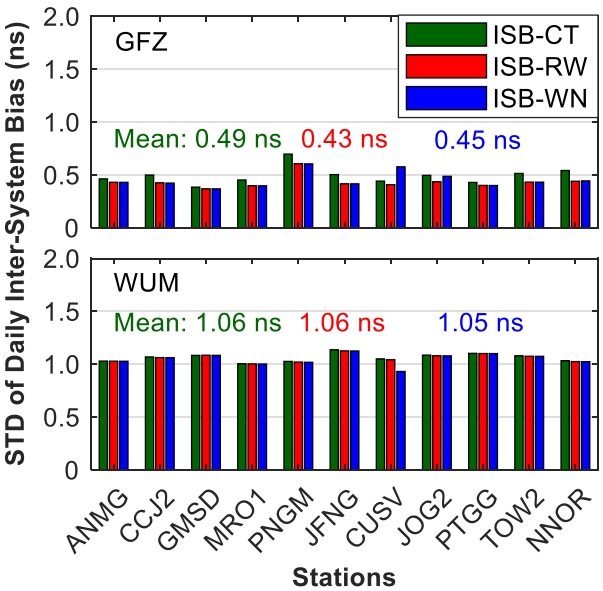

FIGURE 15. STDs of daily ISB over the whole analysis period (11 days) under different ISB handling strategies using GFZ and WUM final products at 11 MGEX stations.

WUM products (actually, it is indicated that the performance difference is marginal for the three different ISB estimation strategies), and estimated as random walk process when

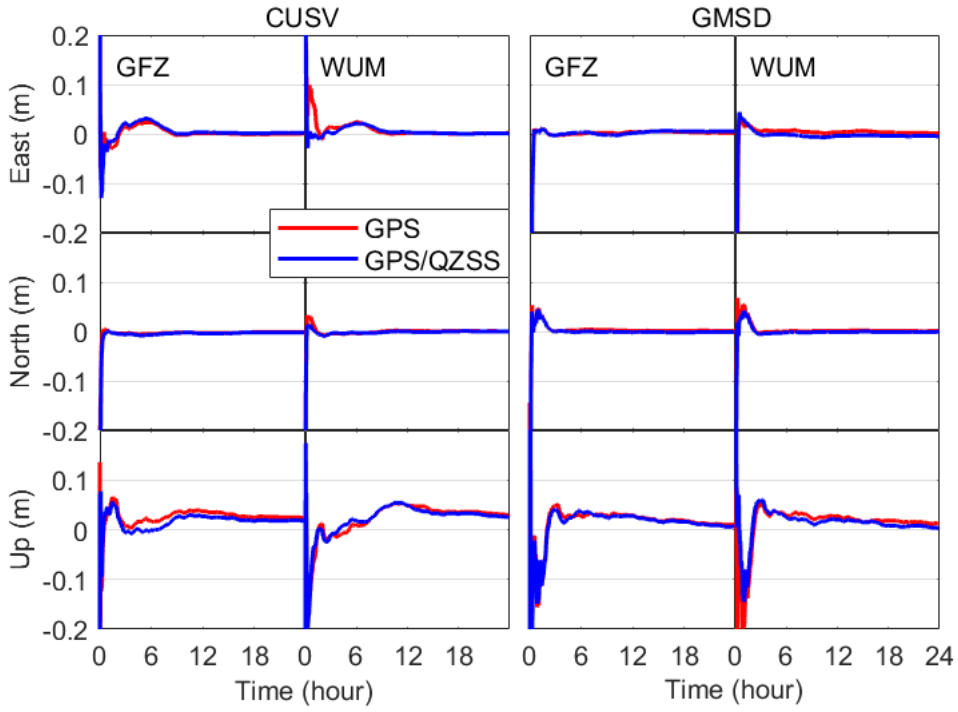

FIGURE 16. Epoch-wise position errors for GPS-only and GPS/QZSS PPP with GFZ and WUM precise products at CUSV and GMSD stations on 5 December 2019.

using GFZ products. Figure 16 depicts the positioning error series of GPS/QZSS PPP at CUSV and GMSD stations on 5 December 2019. For comparison, the results of GPS-only PPP are also presented. Under the cut-off elevation of 30°, the introduction of QZSS observations can improve the positioning performance, especially in the east and up directions. For each 24-h session, the RMS value of the positioning errors in the last half hour is calculated, and the average values of all the stations for 11 consecutive days are further calculated (see Table 5). The fully converged positioning accuracy of GPS-only PPP with GFZ and WUM products at an elevation mask of 30° can be 0.7, 0.3 and 1.9 cm, and 0.6, 0.3 and 2.1 cm in the east, north and up directions, respectively. The GPS/QZSS combined PPP slightly improves the positioning accuracy to 0.6, 0.2 and 1.7 cm (using GFZ products), and 0.4, 0.3 and 1.9 cm (using WUM products) in the three directions, respectively. Table 5 also provides the availability results of position solutions. The availability refers to the percentage of the number of epochs at which the position solutions can be obtained over the total number of epochs. The availability of GPS-only PPP at a cut-off elevation of 30° is approximately 92%, while the corresponding availability is increased to about 100% after an integration with QZSS.

Actually, the improvement on the positioning performance at high elevation angles, which benefits from the integration with QZSS, is mainly reflected in the aspect of convergence time. Figures 17 and 18 show the distribution of convergence time of GPS/QZSS PPP using GFZ and WUM products, respectively. The cut-off elevation angle is 30° and the corresponding GPS-only PPP results are also given. The

TABLE 5. RMSs of position errors in the last half hour and the availability for GPS-only and GPS/QZSS PPP with different precise products based on the datasets from 11 stations spanning 11 days.

Products	Item	GPS	GPS/QZSS
GFZ	East (cm)	0.7	0.6
	North (cm)	0.3	0.2
	Up (cm)	1.9	1.7
	Ava. (%)	91.7	99.7
WUM	East (cm)	0.6	0.4
	North (cm)	0.3	0.3
	Up (cm)	2.1	1.9
	Ava. (%)	91.5	99.8

average results over all the 24-hour sessions are also provided in each panel. Using GFZ products, the average convergence time of GPS-only PPP is 37.0 min in the up direction, while GPS/QZSS PPP reduces the corresponding convergence time by 18% over the GPS-only case to 30.2 min. Using WUM products, the average convergence time of GPS-only PPP is 24.6, 5.3 and 35.0 min in the east, north and up coordinate components, respectively, and the convergence time improvement is 40%, 8% and 27% after inclusion of QZSS observations in the three components, respectively. The GPS/QZSS PPP with WUM products at an elevation mask of 30° has an average convergence time of 14.7, 4.9 and 25.6 min in the three components, respectively. Regarding the average 3D convergence time, it is 42.9 and 37.4 min for GPS-only and GPS/QZSS PPP using GFZ products, respectively, while the corresponding statistic with WUM products is reduced to 41.7 and 29.0 min, respectively.

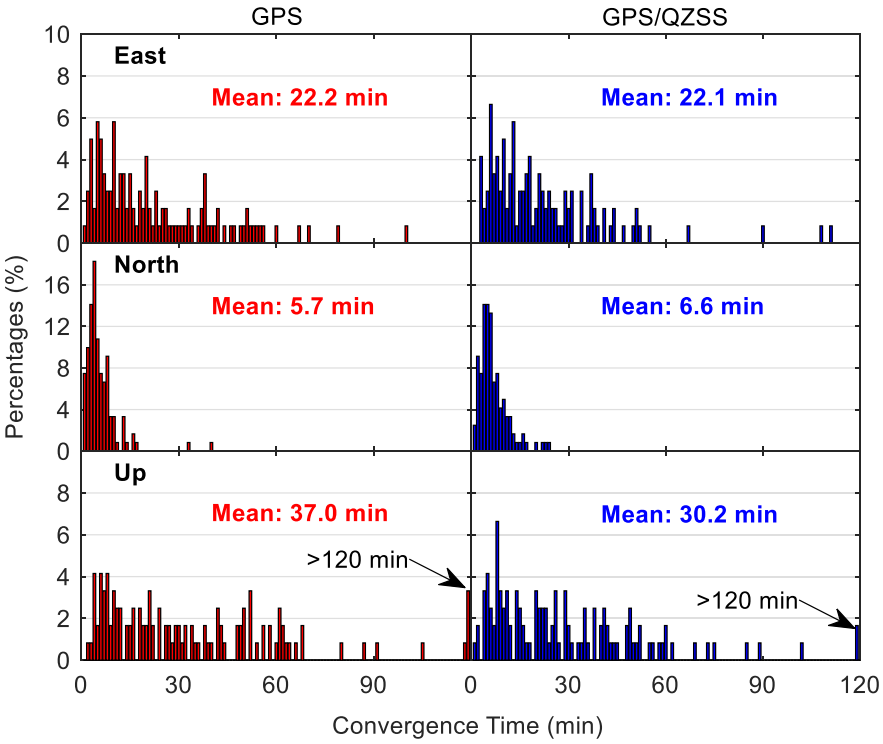

FIGURE 17. Distribution of convergence time for GPS-only and GPS/QZSS PPP using GFZ final products under the elevation mask angle of 30° based on the datasets from 11 stations spanning 11 days.

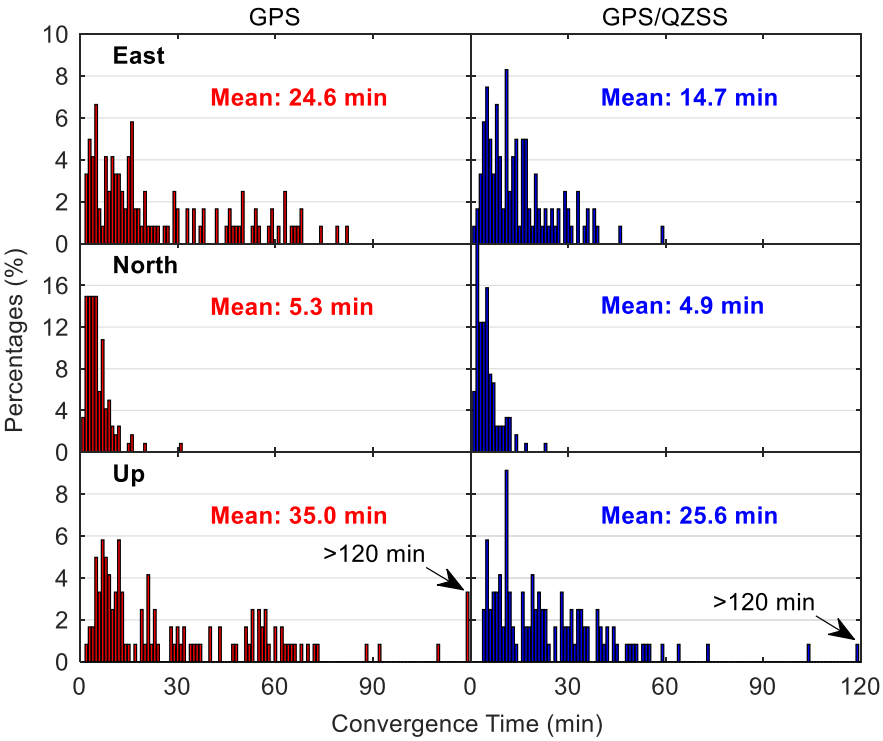

FIGURE 18. Distribution of convergence time for GPS-only and GPS/QZSS PPP using WUM final products under the elevation mask angle of 30° based on the datasets from 11 stations spanning 11 days.

D. POST-PROCESSED KINEMATIC POSITION SOLUTIONS

In addition to the post-processed static PPP mode, the real-time kinematic PPP mode can also be applied to various position service fields. However, it is impossible to conduct the real-time kinematic QZSS-only PPP processing, as both the real-time precise products and the satellite corrections

delivered by the QZSS L6 signal (i.e., the centimeter level augmentation service of QZSS) usually cannot support all the four available QZSS satellites. For completeness, the performance of QZSS-only, GPS-only and GPS/QZSS kinematic PPP in the post-processed mode is analyzed in this section. As the static PPP solutions involved with QZSS observations using WUM products outperform those using GFZ products, the WUM products are used for kinematic PPP processing. As shown in Figures 9, 10 and 11 as well as Table 4, the GPS/QZSS static PPP with the ISB-RW strategy achieves satisfactory position solutions. Thus, the ISB-RW strategy (i.e., estimating ISB as random walk process) is employed for GPS/QZSS kinematic PPP processing in this section. The cut-off elevation angle is set to 7°, and the receiver coordinates are estimated as white noise process.

As there are only four available QZSS satellites at present, QZSS just has preliminary standalone navigation and positioning capability. In addition, the inter-epoch constraints for the receiver coordinates are absent in the kinematic mode. Thus, the reliability and stability of QZSS-only kinematic PPP solutions will not be satisfactory. Figure 19 illustrates the epoch-wise position errors of QZSS-only post-processed PPP under the elevation mask angle of 7° in the kinematic mode at station GMSD on 10 December 2019. The re-convergence repeatedly occurs in the position filter of QZSS-only kinematic PPP. Despite this, when the position filter converges, a decimeter-level positioning accuracy can still be achieved for the QZSS-only kinematic PPP.

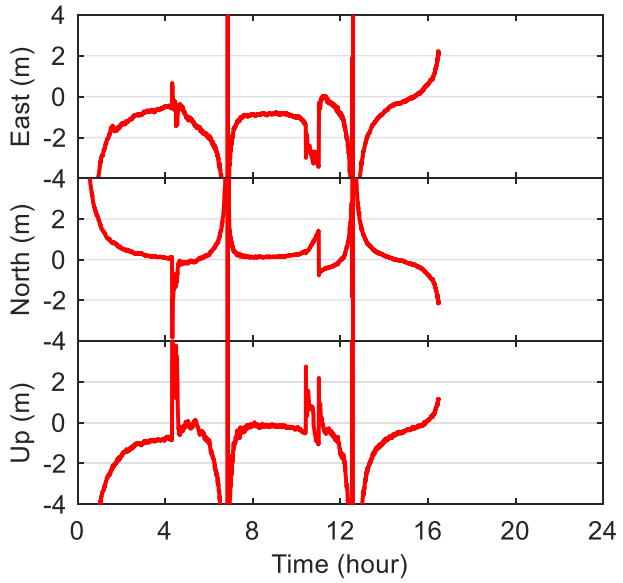

FIGURE 19. Epoch-wise position errors of QZSS-only post-processed PPP under the elevation mask angle of 7° in the kinematic mode at station GMSD on 10 December 2019.

Figure 20 provides the corresponding positioning results of GPS-only and GPS/QZSS kinematic PPP. By contrast, there are no re-convergences in the position filter of GPS-only and GPS/QZSS kinematic PPP. When the position filter converges, the epoch-wise position errors are usually smaller than 5, 5 and 20 cm for both GPS-only and GPS/QZSS kinematic PPP in the east, north and up directions, respectively. In addition, the GPS/QZSS kinematic PPP can slightly reduce the epoch-wise position errors over the GPS-only case, especially for the up direction.

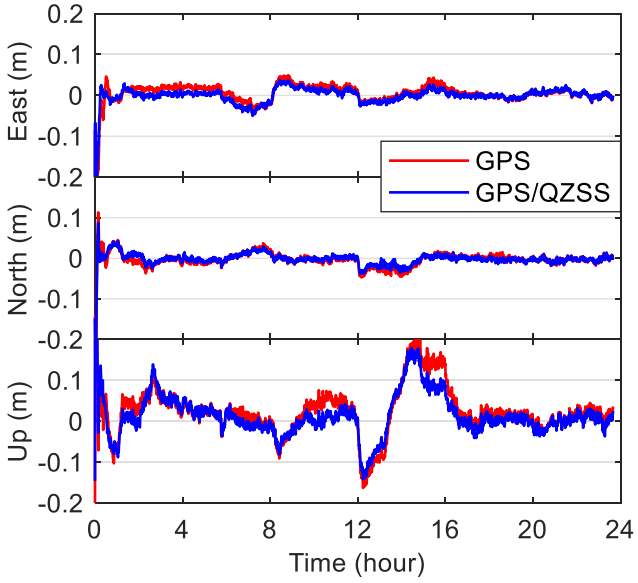

FIGURE 20. Epoch-wise position errors of GPS-only and GPS/QZSS post-processed PPP under the elevation mask angle of 7° in the kinematic mode at station GMSD on 10 December 2019.

For further analysis, Table 6 lists the statistics of position accuracies and convergence time for post-processed GPS-only and GPS/QZSS kinematic PPP based on the datasets from 11 stations spanning 11 days. To evaluate the kinematic positioning accuracy, the RMS value of epoch-wise position errors in the last two hours of each 24-hour session from all the employed 11 stations and 11 days is calculated. The GPS/QZSS PPP can achieve a kinematic positioning accuracy of 1.8, 1.2 and 4.2 cm in the east, north and up directions, respectively, which is only slightly better than that of GPS-only PPP (by 1–2 mm). Similar to the static PPP solutions, the improvement of dual-system combination on the convergence time in the kinematic mode is also significant. The GPS/QZSS kinematic PPP reduces the average convergence time (over the 121 24-hour sessions) by 26%, 30% and 26% in comparison with the GPS-only case to 19.2, 5.4 and 20.5 min in the three directions, respectively. The average 3D convergence time is 38.2 and 27.7 min for GPS-only and GPS/QZSS kinematic PPP, respectively.

E. REAL-TIME STATIC AND KINEMATIC POSITION SOLUTIONS WITH L6E ORBIT AND CLOCK CORRECTIONS

The centimeter level augmentation service broadcast by the L6 signal is a distinctive feature of QZSS. As the performance of real-time PPP with the use of satellite orbit and clock corrections delivered by the QZSS L6 signal draws an increasing

TABLE 6. Statistics of position accuracies and convergence time for post-processed GPS-only and GPS/QZSS kinematic PPP based on the datasets from 11 stations spanning 11 days.

System Combination	Direction	Position Accuracies (cm)	Convergence Time (min)
GPS	East	1.9	26.1
	North	1.4	7.7
	Up	4.3	27.6
GPS/QZSS	East	1.8	19.2
	North	1.2	5.4
	Up	4.2	20.5

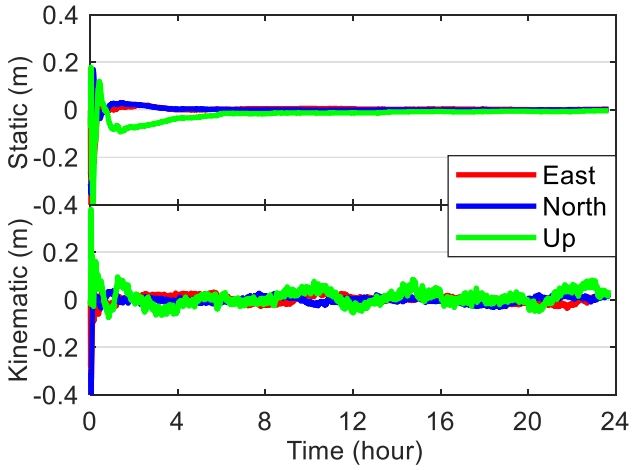

FIGURE 21. Epoch-wise position errors of GPS/QZSS real-time PPP under the elevation mask angle of 7° in the static and kinematic modes at station GMSD on 10 December 2019.

attention from the satellite system users, it is assessed in this section. For ease of scientific research, the Japan Aerospace Exploration Agency (JAXA) provides the archived files of L6E corrections. The real-time precise satellite orbits and clocks can be retrieved by applying the L6E corrections to the broadcast satellite orbits and clocks. As the L6E corrections only supported a QZSS satellite during the analysis period, the QZSS-only real-time PPP solutions cannot be obtained, and the GPS-only real-time PPP solutions are almost the same as those of GPS/QZSS one. Thus, only the GPS/QZSS real-time PPP solutions are provided in this section. The ISB-RW strategy is adopted for GPS/QZSS real-time PPP processing, and the elevation mask angle is set to 7°.

Figure 21 illustrates the epoch-wise position errors of GPS/QZSS real-time PPP under the elevation mask angle of 7° in the static and kinematic modes at station GMSD on 10 December 2019. The position filters of real-time PPP using L6E orbit and clock corrections can also converge to a centimeter-level accuracy after a processing time of tens of minutes in both static and kinematic modes. For further analysis, Table 7 lists the statistics of position accuracies and convergence time for GPS/QZSS real-time static and kinematic PPP based on the datasets from 11 stations spanning 11 days. According to the RMS value of epoch-wise position errors in the last half hour (for static solutions) and last two hours (for kinematic solutions) of each 24-hour session from all the employed 11 stations and 11 days, the GPS/QZSS real-time PPP can achieve a positioning accuracy of 1.2, 1.2 and 1.4 cm in the static mode, and of 2.7, 2.6 and 7.3 cm in the kinematic mode in the east, north and up directions, respectively, which is worse than that of GPS/QZSS post-processed PPP (see Tables 4 and 6). The average convergence time (over the 121 24-hour sessions) for the GPS/QZSS real-time PPP is 14.3, 4.2 and 14.5 min in the static mode, and 23.3, 8.7 and 24.8 min in the kinematic mode in the three directions, respectively, which is comparable to that of GPS/QZSS post-processed PPP (see Figures 10 and 11, and Table 6). Regarding the 3D convergence time of GPS/QZSS real-time PPP, the average value is 18.3 and 34.7 min in the static and kinematic modes, respectively.

TABLE 7. Statistics of position accuracies and convergence time for GPS/QZSS real-time static and kinematic PPP based on the datasets from 11 stations spanning 11 days.

Mode	Direction	Position Accuracies (cm)	Convergence Time (min)
Static	East	1.2	14.3
	North	1.2	4.2
	Up	1.4	14.5
Kinematic	East	2.7	23.3
	North	2.6	8.7
	Up	7.3	24.8

VI. SUMMARY AND CONCLUSION

QZSS has formed a four-satellite constellation, and thus has preliminary standalone navigation and positioning capability. This paper mainly focuses on the current positioning performance of QZSS-only PPP, and also carries out a comparison with the corresponding results of GPS-only PPP. For completeness, the positioning performance of GPS/QZSS combined PPP is also analyzed. Based on the datasets from 11 MGEX tracking stations on 11 consecutive days, the derived results are summarized as follows:

(1) Different from the GPS satellites, the PIFCB of QZSS satellites is not significant. Thus, the multi-frequency data processing becomes easy for QZSS. The PMN errors of QZSS satellites are at the same level as GPS Block IIF satellites, and decrease from 10 to 2 mm with increasing elevation angles from 10° to zenith.

(2) The fully converged positioning accuracy of static QZSS-only PPP in a post-processing mode is approximately 4, 2 and 15 cm in the east, north and up coordinate directions, respectively. The convergence time of QZSS-only PPP using WUM products is significantly shorter than that using GFZ products, and the average value with a convergence threshold of 2 dm in the up direction and 1 dm in the east and north directions is 75.2, 44.3 and 45.6 min in the three coordinate components, respectively. Due to the limited

number of available satellites, the positioning performance of QZSS-only PPP is far worse than that of GPS-only PPP.

(3) The influence of the dynamic models of ISB parameters between GPS and QZSS on the GPS/QZSS integrated PPP processing is comprehensively evaluated. The results indicate that it is not recommended to ignore ISB or estimate it as constants (ISB-IN or ISB-CT) when using GFZ products. In these two cases, both the positioning accuracy and convergence time of GPS/QZSS PPP are even much worse than those of GPS-only PPP. When using WUM products, the derived results with various ISB estimation strategies do not exhibit obvious difference among each other, but ISB-CT is the best strategy in terms of the convergence time. As for the stability of ISB, the short-term stability of the estimated ISB using GFZ products is not as good as that using WUM products. The STD values of epoch-wise ISB over a day using WUM products under the strategies of ISB-CT, ISB-RW and ISB-WN are 0.18, 0.18 and 0.23 ns, respectively. However, the long-term stability of the estimated ISB using GFZ products is better than that using WUM products. The STD values of daily ISB (i.e., the average value of epoch-wise ISB over a day) over the whole analysis period (11 days) using GFZ products under the three different ISB estimation strategies are 0.49, 0.43 and 0.45 ns, respectively. In addition, except for two stations equipped with TRIMBLE NETR9 receiver, the daily ISB is consistent for the stations with the same type of receivers.

(4) In harsh environments, compared with post-processed GPS-only static solutions, the integration of QZSS and GPS slightly improves the positioning accuracy and the availability, and the main improvements are reflected in the aspect of convergence time. At a cut-off elevation angle of 30°, compared with GPS-only PPP, the convergence time of GPS/QZSS PPP using GFZ products is reduced by 18% in the up direction, and the corresponding convergence time using WUM products is decreased by 40%, 8% and 27% in the east, north and up coordinate components, respectively.

(5) Due to the limited available satellites, the re-convergence repeatedly occurs in the position filter of post-processed QZSS-only kinematic PPP, but a decimeter-level positioning accuracy can still be achieved when the position filter converges. Similar to the static PPP solutions, the improvement of dual-system combination over post-processed GPS-only kinematic PPP is marginal on positioning accuracy, but can be several minutes on convergence time.

(6) With the use of L6E orbit and clock corrections, the GPS/QZSS real-time PPP can achieve a positioning accuracy of 1.2, 1.2 and 1.4 cm in the static mode, and of 2.7, 2.6 and 7.3 cm in the kinematic mode in the east, north and up directions, respectively, which is worse than that of GPS/QZSS post-processed PPP. The average convergence time for the GPS/QZSS real-time PPP is 14.3, 4.2 and 14.5 min in the static mode, and 23.3, 8.7 and 24.8 min in the kinematic mode in the three directions, respectively, which is comparable to that of GPS/QZSS post-processed PPP.

In general, although there are only four available satellites from QZSS at present, an acceptable static positioning performance of standalone PPP can still be obtained. Better precise positioning services in the Asia-Pacific regions can be expected when QZSS is extended to a seven-satellite constellation.

REFERENCES

[1] A. Hauschild, P. Steigenberger, and C. Rodriguez-Solano, "Signal, orbit and attitude analysis of Japan's first QZSS satellite Michibiki," *GPS Solutions*, vol. 16, no. 1, pp. 127–133, Jan. 2012.

[2] Y. Quan, L. Lau, G. W. Roberts, and X. Meng, "Measurement signal quality assessment on all available and new signals of multi-GNSS (GPS, GLONASS, Galileo, BDS, and QZSS) with real data," *J. Navig.*, vol. 69, no. 2, pp. 313–334, Mar. 2016.

[3] F. Zhou, D. Dong, P. Li, X. Li, and H. Schuh, "Influence of stochastic modeling for inter-system biases on multi-GNSS undifferenced and uncombined precise point positioning," *GPS Solutions*, vol. 23, no. 3, p. 59, Jul. 2019.

[4] S. Zhu, D. Yue, L. He, Z. Liu, and J. Chen, "Comprehensive analysis of compatibility between QZSS and GPS in Asia–Pacific region: Signal quality, RTK and PPP," *Adv. Space Res.*, vol. 66, no. 2, pp. 395–411, Jul. 2020.

[5] W. Xie, G. Huang, B. Cui, P. Li, Y. Cao, H. Wang, Z. Chen, and B. Shao, "Characteristics and performance evaluation of QZSS onboard satellite clocks," *Sensors*, vol. 19, no. 23, p. 5147, Nov. 2019.

[6] F. Guo, X. Li, X. Zhang, and J. Wang, "Assessment of precise orbit and clock products for Galileo, BeiDou, and QZSS from IGS multi-GNSS experiment (MGEX)," *GPS Solutions*, vol. 21, no. 1, pp. 279–290, Jan. 2017.

[7] X. Li, Y. Zhu, K. Zheng, Y. Yuan, G. Liu, and Y. Xiong, "Precise orbit and clock products of Galileo, BDS and QZSS from MGEX since 2018: Comparison and PPP validation," *Remote Sens.*, vol. 12, no. 9, p. 1415, Apr. 2020.

[8] K. Sośnica, R. Zajdel, G. Bury, J. Bosy, M. Moore, and S. Masoumi, "Quality assessment of experimental IGS multi-GNSS combined orbits," *GPS Solutions*, vol. 24, no. 2, p. 54, Apr. 2020.

[9] X. Li, Y. Yuan, J. Huang, Y. Zhu, J. Wu, Y. Xiong, X. Li, and K. Zhang, "Galileo and QZSS precise orbit and clock determination using new satellite metadata," *J. Geodesy*, vol. 93, no. 8, pp. 1123–1136, Aug. 2019.

[10] Y. Zhang, N. Kubo, J. Chen, H. Wang, and J. Wang, "Assessment of the contribution of QZSS combined GPS/BeiDou positioning in Asia–Pacific areas," in *Proc. China Satell. Navig. Conf. (CSNC)*, Shanghai, China, 2018, pp. 467–478.

[11] J. Bu, X. Zuo, X. Li, J. Chang, and X. Zhang, "Evaluation and analysis on positioning performance of BDS/QZSS satellite navigation systems in Asian–Pacific region," *Adv. Space Res.*, vol. 63, no. 7, pp. 2189–2211, Apr. 2019.

[12] J. Hong, R. Tu, R. Zhang, L. Fan, P. Zhang, and J. Han, "Contribution analysis of QZSS to single-frequency PPP of GPS/BDS/GLONASS/Galileo," *Adv. Space Res.*, vol. 65, no. 7, pp. 1803–1817, Apr. 2020.

[13] J. Hu, X. Zhang, P. Li, F. Ma, and L. Pan, "Multi-GNSS fractional cycle bias products generation for GNSS ambiguity-fixed PPP at Wuhan university," *GPS Solutions*, vol. 24, no. 1, p. 15, Jan. 2020.

[14] J. Geng, J. Guo, X. Meng, and K. Gao, "Speeding up PPP ambiguity resolution using triple-frequency GPS/BeiDou/Galileo/QZSS data," *J. Geodesy*, vol. 94, no. 1, p. 6, Jan. 2020.

[15] S. Choy, K. Harima, Y. Li, M. Choudhury, C. Rizos, Y. Wakabayashi, and S. Kogure, "GPS precise point positioning with the Japanese quasi-Zenith satellite system LEX augmentation corrections," *J. Navigat.*, vol. 68, no. 4, pp. 769–783, Jul. 2015.

[16] S. Zhang, S. Du, W. Li, and G. Wang, "Evaluation of the GPS precise orbit and clock corrections from MADOCA real-time products," *Sensors*, vol. 19, no. 11, p. 2580, Jun. 2019.

[17] X. Li, L. Pan, W. Yu, W. Dai, Y. Li, and H. Peng, "A comprehensive assessment of four-satellite QZSS constellation: Navigation signals, broadcast ephemeris, availability, SPP, interoperability with GPS, and ISB against GPS," *Surv. Rev.*, early access, pp. 1–17, Dec. 2020, doi: 10.1080/00396265.2020.1858256.

[18] S. Zaminpardaz, K. Wang, and P. J. G. Teunissen, "Australia-first high-precision positioning results with new Japanese QZSS regional satellite system," *GPS Solutions*, vol. 22, no. 4, p. 101, Oct. 2018.

[19] T. Takasu and A. Yasuda, "Development of the low-cost RTK-GPS receiver with an open source program package RTKLIB," in *Proc. Int. Symp. GPS/GNSS*, Jeju, South Korea, Nov. 2009, pp. 1–6.

[20] L. Pan, X. Zhang, X. Li, J. Liu, and X. Li, "Characteristics of inter-frequency clock bias for block IIF satellites and its effect on triple-frequency GPS precise point positioning," *GPS Solutions*, vol. 21, no. 2, pp. 811–822, Apr. 2017.

[21] O. Montenbruck, A. Hauschild, P. Steigenberger, U. Hugentobler, P. Teunissen, and S. Nakamura, "Initial assessment of the COMPASS/BeiDou-2 regional navigation satellite system," *GPS Solutions*, vol. 17, no. 3, pp. 211–222, Apr. 2013.

XUANPING LI was born in Changsha, Hunan, China, in 1997. He received the bachelor's degree from China University of Geosciences, in 2019. He is currently pursuing the master's degree with the School of Geosciences and Info-Physics, Central South University, China. His main research interest includes GNSS precise positioning.

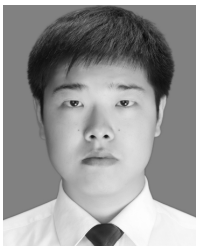

LIN PAN was born in Dingzhou, Hebei, China, in 1989. He received the Ph.D. degree in geodesy and engineering surveying from Wuhan University, in 2018. He is currently an Associate Professor with Central South University. His current research interest includes GNSS precise positioning.

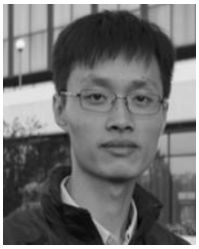

WENKUN YU received the Ph.D. degree from The Hong Kong Polytechnic University, in 2019. He is currently an Assistant Professor with the School of Geosciences and Info-physics, Central South University, China. His main research interests include BeiDou/GNSS high-precision positioning and applications for deformation monitoring.